forced to differentiate in response to retinoic acid (RA) [10]. RA has been shown to play an important role in early embryonic development and in the generation of several systems such as nervous system [11]. Based on these findings, RA-mediated terminal differentiation of neuroblastoma is used as a current standard therapy for the high-risk neuroblastoma, however, a precise molecular basis underlying neuroblastoma differentiation has been elusive.

To understand a molecular mechanism(s) behind the genesis as well as the aggressive progression of neuroblastoma, we have identified a large number of genes expressed differentially between favorable and unfavorable neuroblastomas [12]. NLRR3 is one of NLRR family of type I transmembrane protein with the typical leucine-rich repeat (LRR) domain, and its expression level was extremely higher in favorable neuroblastomas than that in unfavorable ones, indicating that *NLRR3* expression might be one of favorable prognostic indicators in neuroblastoma [12,13]. Recently, we have found that MYCN has an ability to repress the transcription of *NLRR3* through the functional collaboration with Miz-1, raising a possibility that MYCN-induced down-regulation of NLRR3 contributes at least in part to the aggressive phenotype of the high-risk neuroblastoma [14]. However, the precise molecular event(s) and mechanism(s) involved remain unclear.

In this study, we have found that the intracellular fragment of NLRR3 (NLRR3-ICD) plays a pivotal role in the regulation of ATRA (all-*trans* retinoic acid)-mediated neuroblastoma differentiation.

2. Materials and methods

2.1. Cell lines

Human neuroblastoma SK-N-BE, SH-SY5Y and TGW cells were grown in RPMI 1640 medium (Sigma) supplemented with 10% heat-inactivated fetal bovine serum (Invitrogen), 100 units/ml of penicillin and 100 μg/ml of streptomycin. Cells were grown at 37 °C in a humidified incubator with 5% CO_2. For neuroblastoma differentiation experiments, SH-SY5Y cells were exposed to 5 μM of all-*trans* retinoic acid (ATRA; Sigma).

2.2. Clinical samples

Patient samples were collected with patients' written informed consent in accordance with ethics approval obtained from the internal review board.

2.3. Transfection

Cells were transfected with the indicated expression plasmids using LipofectAMINE 2000 (Invitrogen) according to the manufacturer's instructions.

2.4. Deletion constructs of NLRR3

The expression plasmids encoding human NLRR3 (1–708), NLRR3-ECD (1–649), NLRR3-ECD-sol (1–628), NLRR3-d-ECD (629–708) or NLRR3-ICD (648–708) were generated by PCR-based amplification. PCR products were gel-purified and inserted into the appropriate restriction sites of pcDNA3.1 expression plasmid (Invitrogen) with COOH-terminal HA epitope tag to give pcDNA3.1-NLRR3, pcDNA3.1-NLRR3-ECD, pcDNA3.1-NLRR3-ECD-sol, pcDNA3.1-NLRR3-d-ECD and pcDNA3.1-NLRR3-ICD. The nucleotide sequences of these expression plasmids were verified by DNA sequencing.

2.5. Cell survival assay

Cells were seeded at a density of 1.0×10^3 cells/96-well plates and allowed to attach overnight. Cells were then maintained in standard culture medium, and visualized using a real-time cell imaging system (IncuCyte; Essen's Bioscience) according to the manufacturer's recommendations.

2.6. Colony formation assay

SK-N-BE or TGW cells were seeded at a density of 2.0×10^3 cells/6-well plates, and then transfected with the indicated expression plasmids. Forty-eight hours after transfection, cells were transferred to the fresh medium containing G418 (600 μg/ml). After 14 days of the incubation, G418-resistant colonies were fixed in methanol, and stained with Giemsa's solution.

2.7. Immunoprecipitation

Equal amounts of cell lysates (1 mg of protein) were precleared with 20 μl of protein A-Sepharose beads (GE Healthcare) and subjected to immunoprecipitation with anti-NLRR3 or with anti-HA antibody (Roche). The immunoprecipitates were then analyzed by immunoblotting with anti-NLRR3 or with anti-HA antibody. ECL (enhanced chemiluminescence; GE Healthcare) was used to detect the presence of immuno-reactive bands.

2.8. Immunohistochemistry

Paraffin-embedded sympathetic ganglia tissues were fixed in 10% formaldehyde and then incubated with anti-NLRR3 antibody. Immunohistochemical analysis was performed as described [14].

2.9. Immunofluorescence

Cells were grown on glass coverslips in standard culture medium. Cells were washed in PBS, fixed in 4% paraformaldehyde for 20 min at 4 °C, permeabilized with 0.1% Triton X-100 for 20 min at room temperature, and then blocked with 1% BSA plus 5% goat serum for 1 h at room temperature. After blocking, cells were incubated with anti-HA, anti-NLRR3, anti-Tuj-1 antibody (Covance) or with a normal rabbit IgG for 1 h at room temperature, followed by the incubation with Alexa Fluor 546-conjugated goat anti-rabbit IgG (Life Technologies). Cell nuclei were stained with DAPI. The coverslips were mounted into glass slides, and images were captured using a confocal laser scanning microscope (Leica).

2.10. Statistical analysis

All values were expressed as the means ± SEM. One-way ANOVA with a post hoc Dunnett's test were used to determine level of significance for colony formation assay and percentage of differentiated cells ($^{**}P < 0.01$). Two-way ANOVA followed by a multiple comparison post hoc Bonferroni's test was used to compare differences between groups in cell viability assay ($^{*}P < 0.05$ and $^{**}P < 0.01$).

3. Results

3.1. Induction of NLRR3-related peptide during ATRA-mediated neuroblastoma differentiation

To examine the expression pattern of NLRR3 during ATRA (all-*trans* retinoic acid)-dependent neuroblastoma differentiation, human neuroblastoma SH-SY5Y cells were exposed to 5 μM of

ATRA. At the indicated time periods after treatment, cell lysates were subjected to immunoprecipitation/immunoblotting with anti-NLRR3 antibody. Consistent with our recent findings [14], an obvious elongation of neurite (one of the hallmark processes of neuronal morphological differentiation) was observed in ATRA-treated SH-SY5Y cells in a time-dependent manner (Fig. 1A). It is worth noting that ATRA promotes a remarkable accumulation of a small peptide which is recognized by anti-NLRR3 antibody (Fig. 1B).

Since anti-NLRR3 antibody was raised against the extreme COOH-terminal intracellular domain of NLRR3 [14], it is possible that, like NICD (Notch intracellular domain) [15], this small peptide is produced by a proteolytic cleavage of NLRR3 in SH-SY5Y cells exposed to ATRA. It has been well-documented that, upon ligand binding, NICD is released from the plasma membrane after proteolytic processing, and thereby translocating into cell nucleus [15]. To test this possibility, we performed the indirect immunofluorescence experiments to examine the subcellular localization of NLRR3 in response to ATRA. At the indicated time points after ATRA treatment, SH-SY5Y cells were fixed and stained with anti-NLRR3 antibody. As shown in Fig. 1C, NLRR3 was extremely detectable outside of cell nucleus in the absence of ATRA. Intriguingly, a small fraction of NLRR3 was clearly induced to accumulate in ATRA-treated cell nucleus in a time-dependent fashion, suggesting that ATRA-mediated proteolysis releases the intracellular domain of NLRR3 from plasma membrane and thereby promoting its nuclear access. Although further experiments should be required to address this issue, we tentatively termed this small peptide NLRR3-ICD (NLRR3 intracellular domain).

3.2. Secretase-dependent proteolytic cleavage of NLRR3 to generate NLRR3-ICD

It has been widely accepted that NICD is generated through the sequential and highly regulated intramembrane proteolysis mediated by three distinct types of proteases including γ-secretase complex [15]. As described [16], γ-secretase cleaves quite a broad range of substrates, and there are no distinct consensus amino acid sequences of intramembrane γ-cleavage sites among them (Fig. 2A). Considering that NLRR3-ICD might be released from the plasma membrane, it is likely that γ-secretase-mediated proteolytic cleavage is involved in the production of NLRR3-ICD. To verify this hypothesis, we took advantage of γ-secretase inhibitor, inhibitor X [17]. SH-SY5Y cells were treated with inhibitor X or left untreated. Twenty-four hours post treatment, cell lysates were analyzed by immunoprecipitation/immunoblotting with anti-NLRR3 antibody. As shown in Fig. 2B, NLRR3-ICD was undetectable in the presence of inhibitor X, indicating that γ-secretase activity is required for the production of NLRR3-ICD.

To further confirm this issue, neuroblastoma SK-N-BE cells were transfected with the expression plasmid for HA-tagged NLRR3, followed by an incubation with or without inhibitor X. The endogenous expression level of NLRR3 in SK-N-BE cells was quite low when compared with that in SH-SY5Y cells (data not shown).

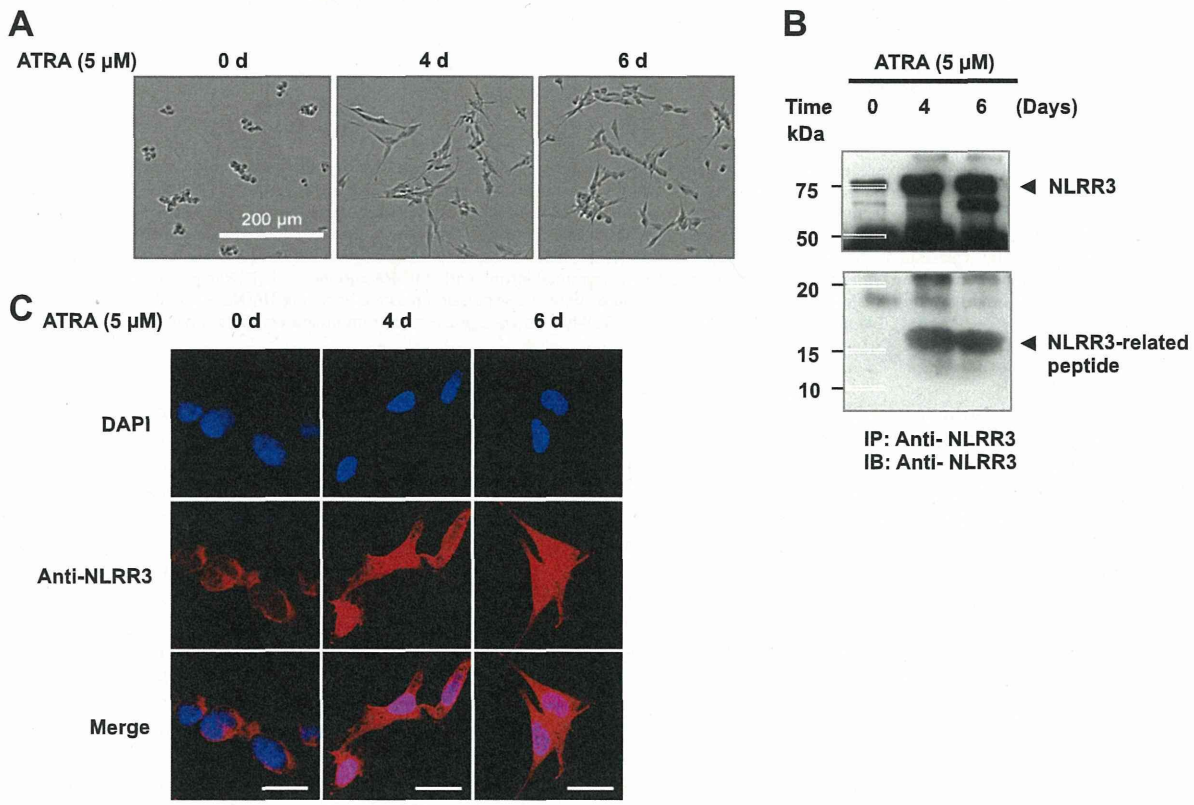

Fig. 1. Accumulation of an NLRR3-related peptide during ATRA-mediated neuroblastoma differentiation. (A) ATRA-mediated neuronal differentiation of neuroblastoma SH-SY5Y cells. SH-SY5Y cells were treated with 5 μM of ATRA. At the indicated time periods after treatment, pictures were taken. Note that ATRA-dependent neurite outgrowth was seen. Scale bar; 200 μm. (B) Expression of NLRR3 in response to ATRA. SH-SY5Y cells were treated as in (A). At the indicated time points after ATRA exposure, cell lysates were analyzed by immunoprecipitation with anti-NLRR3 antibody, followed by immunoblotting with anti-NLRR3 antibody. Arrow heads indicate native NLRR3 and NLRR3-related peptide. (C) ATRA-mediated nuclear access of NLRR3. SH-SY5Y cells were treated as in (A). At the indicated time periods after ATRA treatment, cells were fixed and then probed with anti-NLRR3 antibody, followed by the incubation with Alexa flour 546-conjugated secondary antibody (red). Cells were also stained with DAPI to visualize nuclei (blue). Scale bar; 25 μm. (For interpretation of the references to color in this figure legend, the reader is referred to the web version of this article.)

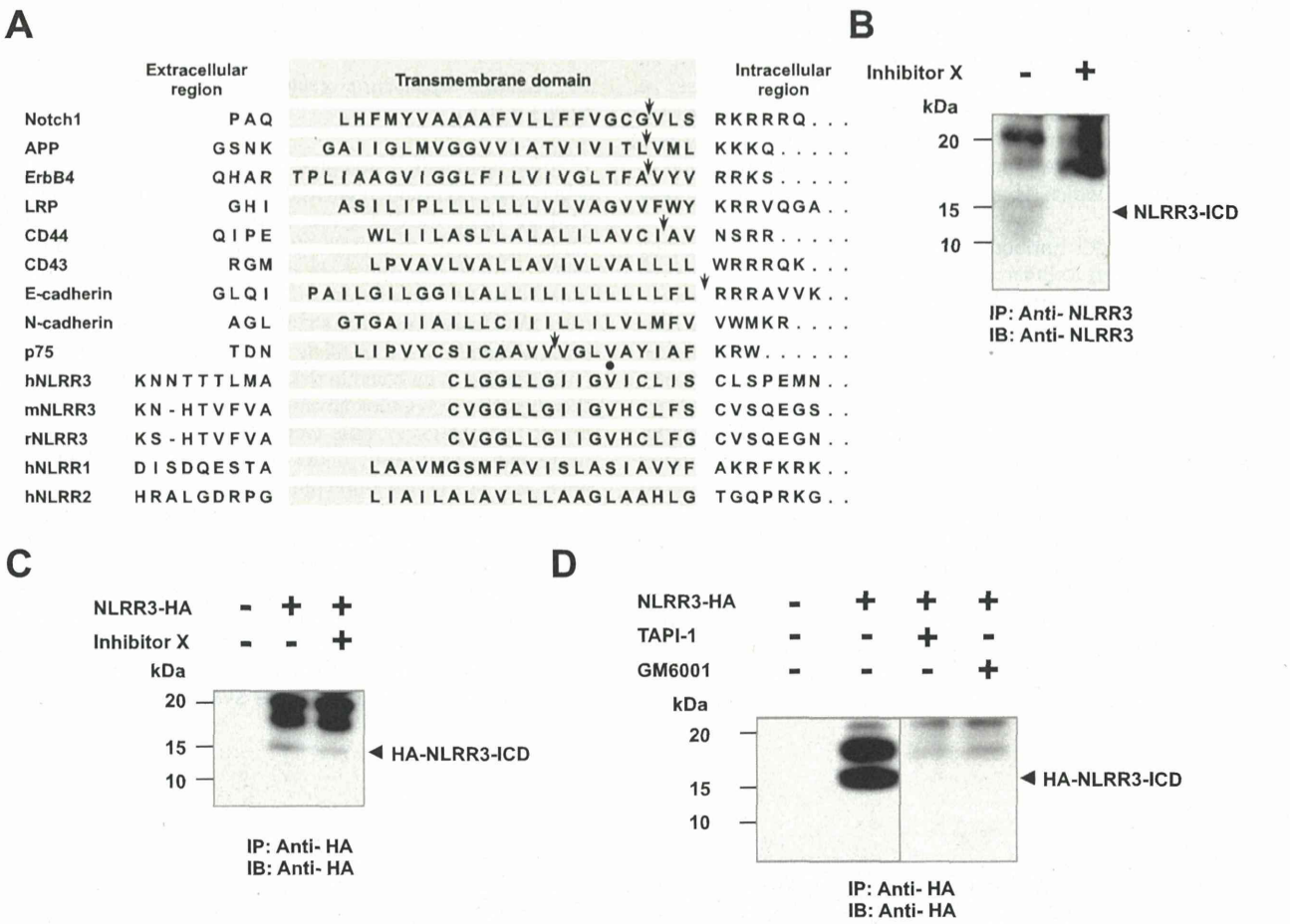

Fig. 2. Production of NLRR3 COOH-terminal peptide (NLRR3-ICD) through the proteolytic cleavage of NLRR3 by α- and γ-secretases. (A) Alignment of the amino acid sequences from transmembrane domains of human γ-secretase substrates. Arrows and filled circle indicate γ-cleavage sites of the indicated substrates and potential γ-cleavage site of NLRR3, respectively. (B and C) γ-secretase inhibitor blocks the production of NLRR3-ICD. SH-SY5Y cells were treated with 1 μM of inhibitor X or left untreated. Twenty-four hours after treatment, cell lysates were immunoprecipitated with anti-NLRR3 antibody, followed by immunoblotting with anti-NLRR3 antibody (B). SK-N-BE cells were transfected with the empty plasmid or with the expression plasmid for HA-NLRR3 and treated with or without inhibitor X. Twenty-four hours after treatment, cell lysates were subjected to immunoprecipitation with anti-HA antibody, followed by immunoblotting with anti-HA antibody (C). (D) The production of NLRR3-ICD is blocked by α-secretase inhibitors. SK-N-BE cells were transfected with the empty plasmid or with the expression plasmid encoding HA-NLRR3, and incubated in the presence or absence of TAPI-1 (20 μM) or GM6001 (10 μM). Twenty-four hours after treatment, cell lysates were processed for immunoprecipitation with anti-HA antibody, followed by immunoblotting with anti-HA antibody.

Twenty-four hours after treatment, cell lysates were analyzed by immunoprecipitation/immunoblotting with anti-HA antibody. As shown in Fig. 2C, the amount of HA-NLRR3-ICD was reduced in cells exposed to inhibitor X. Next, we have introduced the expression plasmid encoding HA-NLRR3 into SK-N-BE cells, and the transfected cells were then exposed to α-secretase inhibitors such as TAPI-1 and GM6001 [18] or left untreated. As clearly seen in Fig. 2D, the generation of HA-NLRR3-ICD was greatly abolished by these inhibitor treatments. Thus, it is highly likely that NLRR3-ICD is produced at least in part through the secretase-dependent proteolytic cleavage of NLRR3.

3.3. Nuclear access of NLRR3-ICD

We next assessed whether NLRR3-ICD could be localized within cell nucleus. SK-N-BE cells were transfected with the expression plasmid for HA-NLRR3. Forty-eight hours post transfection, the transfected cells were biochemically fractionated into cytoplasmic and nuclear fractions, and equal amounts of each fraction were analyzed by immunoblotting with anti-HA antibody. The purity of the cytoplasmic and nuclear fractions were verified by immunoblotting with anti-tubulin-α and anti-lamin B antibodies, respectively. As shown in Fig. 3A, the exogenously expressed HA-NLRR3 underwent proteolytic processing and the resultant HA-NLRR3-ICD was largely detected in nuclear fraction.

To gain further insights into the nuclear distribution of NLRR3-ICD, we have constructed the expression plasmids encoding the indicated HA-NLRR3 deletion mutants (Fig. 3B), and introduced them into SK-N-BE cells. Forty-eight hours after transfection, cells were fixed and probed with anti-HA antibody. As shown in Fig. 3C, HA-NLRR3-ECD and HA-NLRR3-ECD-sol lacking the intracellular domain of NLRR3, exclusively existed outside of cell nucleus, whereas HA-NLRR3-d-ECD containing NLRR3 intracellular domain, was found in both cytoplasm and nucleus. As expected, the nuclear distribution of HA-NLRR3-ICD was observed under our experimental conditions.

Next, we sought to examine whether the nuclear NLRR3 could be also detectable *in vivo*. For this purpose, we have performed an immunohistochemical analysis. Human sympathetic ganglia were fixed in formaldehyde, followed by an incubation with normal rabbit serum or with anti-NLRR3 antibody. As shown in Fig. 3D, anti-NLRR3 antibody recognized the nuclear NLRR3 in sympathetic ganglia, whereas normal rabbit serum did not detect any signals. Together, it appears that NLRR3 is subjected to the

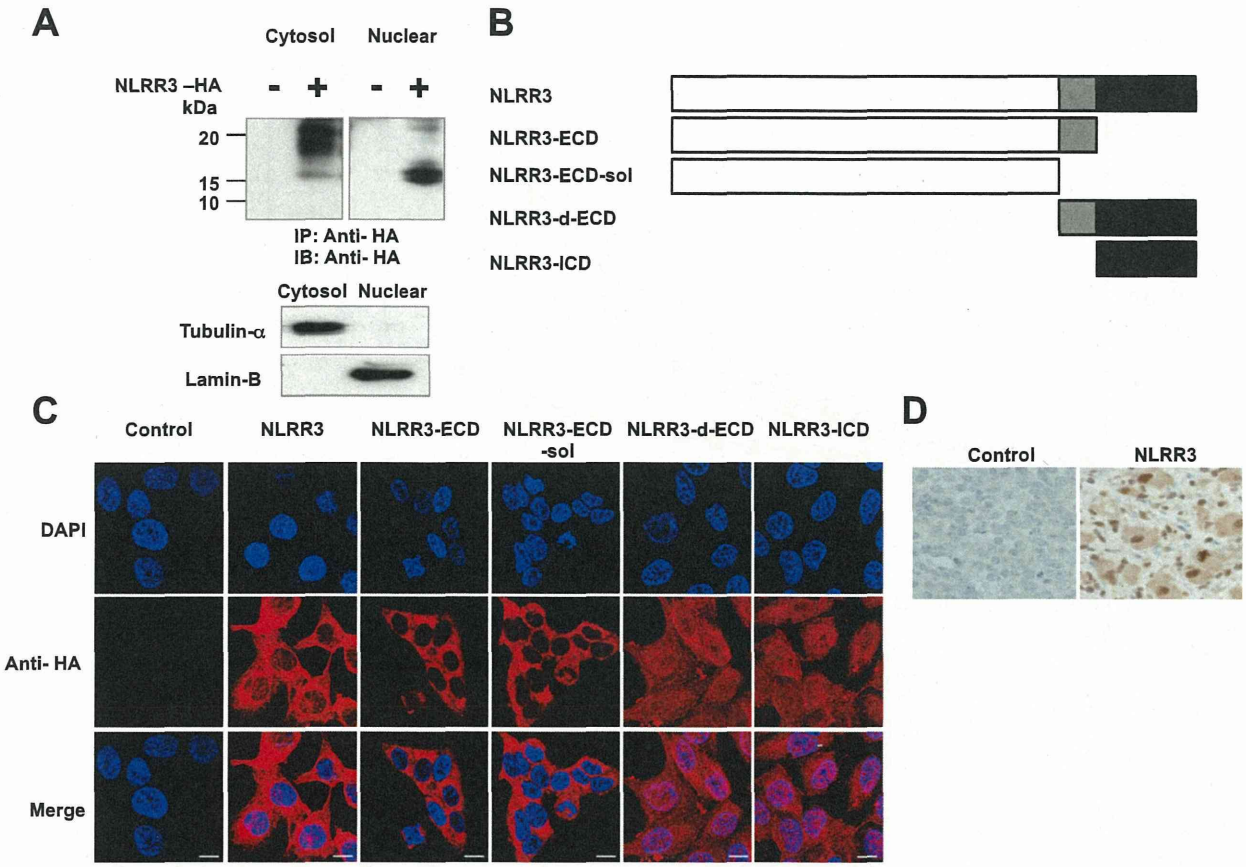

Fig. 3. Nuclear localization of NLRR3-ICD in neuroblastoma cells. (A) Immunoblotting. SK-N-BE cells were transfected with the empty plasmid or with the expression plasmid for HA-NLRR3. Forty-eight hours after transfection, cells were fractionated into cytoplasmic (C) and nuclear (N) fractions. Equal amounts of each fraction were analyzed by immunoblotting with anti-HA (upper panels), anti-Tubulin-α (middle panel), or with anti-Lamin B (lower panel). (B) Schematic diagrams of a full-length NLRR3 and its deletion mutants. Extracellular, transmembrane and intracellular domains of NLRR3 are indicated by open, gray and filled boxes, respectively. (C) Nuclear access of NLRR3-ICD. SK-N-BE cells were transfected with the expression plasmids encoding the above-mentioned HA-NLRR3 derivatives. Forty-eight hours after transfection, cells were fixed and stained with anti-HA antibody (red). Cell nuclei were stained with DAPI (blue). Scale bar; 10 μm. (D) Immunohistochemical staining. Human sympathetic ganglia were incubated with control IgG (left panel) or with anti-NLRR3 antibody (right panel). (For interpretation of the references to color in this figure legend, the reader is referred to the web version of this article.)

proteolytic processing, and thereby translocated from cell membrane to cell nucleus of cultured neuroblastoma cells as well as sympathetic ganglia.

3.4. NLRR3-ICD suppresses neuroblastoma cell proliferation

To explore a possible biological role(s) of NLRR3-ICD, we have examined the effect(s) of the indicated HA-NLRR3 derivatives including HA-NLRR3-ICD on neuroblastoma cell proliferation. SK-N-BE cells stably expressing the indicated HA-NLRR3 derivatives were cultured and their proliferation was monitored by IncuCyte live-cell imaging system. As shown in Fig. 4A, HA-NLRR3, HA-NLRR3-d-ECD and HA-NLRR3-ICD significantly suppressed SK-N-BE cell proliferation as compared with their parental cells. In a sharp contrast, HA-NLRR3-ECD and HA-NLRR3-ECD-sol had an undetectable effect on the rate of proliferation of SK-N-BE cells.

To further evaluate these observations, we have performed colony formation assay. SK-N-BE cells transfected with the indicated HA-NLRR3 derivatives were transferred to the fresh medium containing G418 (600 μg/ml). Two weeks after selection, number of drug-resistant colonies was scored. As shown in Fig. 4B and C, overexpression of HA-NLRR3-d-ECD or HA-NLRR3-ICD resulted in a remarkable decrease in number of drug-resistant colonies as compared with the empty plasmid control cells, whereas HA-NLRR3-ECD and HA-NLRR3-ECD-sol had a marginal effect on number of drug-resistant colonies. Additionally, cells overexpressing HA-NLRR3 showed a modest decrease in the rate of colony formation. Similar results were also obtained in neuroblastoma TGW cells (data not shown). Thus, these results indicate that NLRR3-ICD potentially plays a crucial role in the regulation of neuroblastoma cell proliferation.

3.5. NLRR3-ICD stimulates ATRA-mediated neuroblastoma cell differentiation

Since SH-SY5Y cells showed the remarkable ATRA-induced neurite extension accompanied by the massive accumulation of NLRR3-ICD (Fig. 1A), it is possible that NLRR3-ICD has a capability to trigger or enhance neurite elongation in neuroblastoma cells initiated by ATRA. To address this issue, SK-N-BE cells stably expressing the indicated NLRR3 derivatives were exposed to 1.5 μM of ATRA. Five days after treatment, images were taken and then total neurite outgrowth was assessed. As shown in Fig. 4D and E, an obvious increase in number of cells with neurite extension was observed in HA-NLRR3, HA-NLRR3-d-ECD or HA-NLRR3-ICD-expressing cells relative to that in the empty plasmid control cells. In contrast, HA-NLRR3-ECD and HA-NLRR3-ECD-sol did not have a significant effect on ATRA-mediated neurite outgrowth. Similar

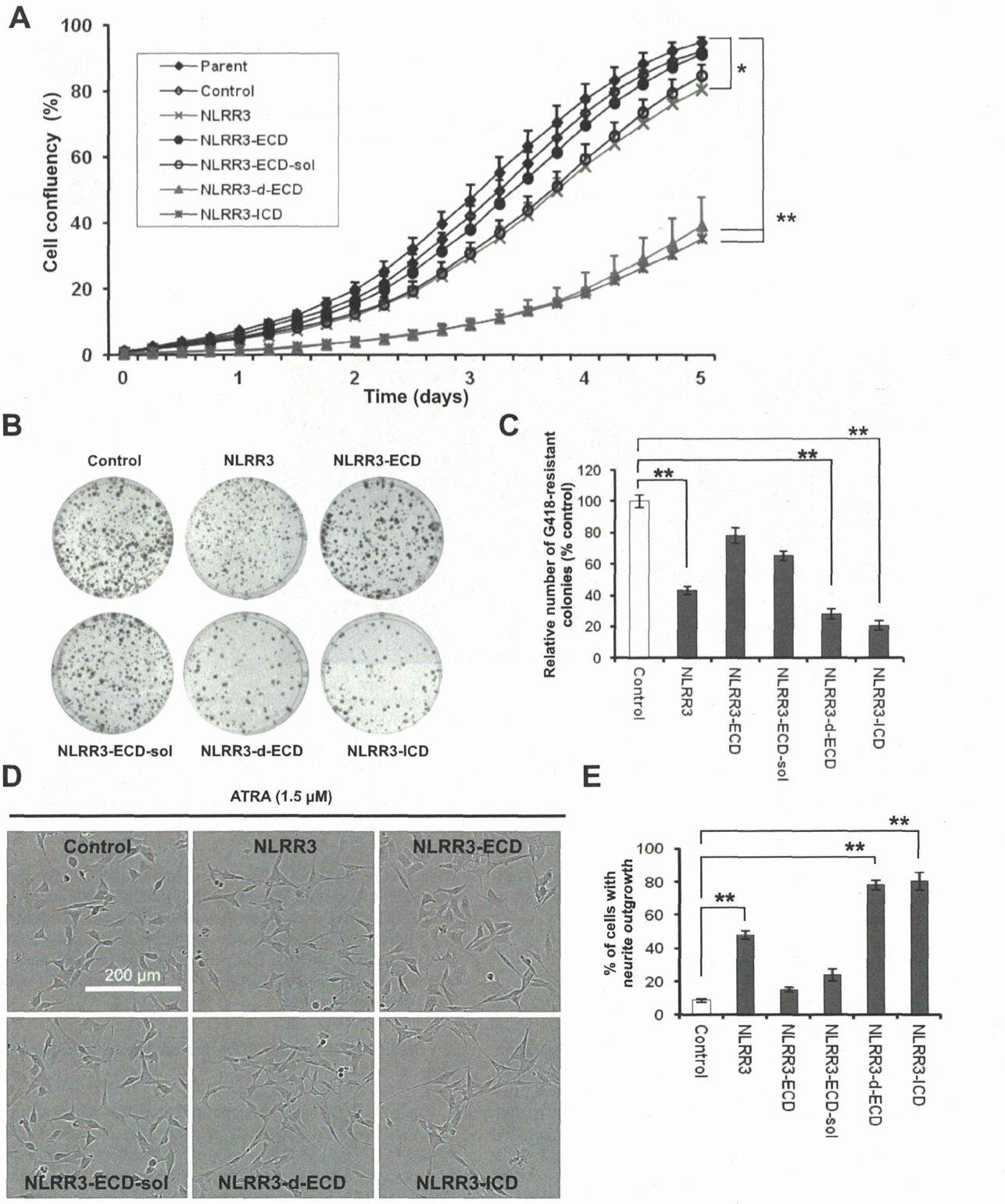

Fig. 4. NLRR3-ICD promotes growth suppression and ATRA-dependent neurite extension of neuroblastoma cells. (A) Growth curves. SK-N-BE cells stably expressing the indicated NLRR3 derivatives were grown in the medium and their growth rates were monitored by IncuCyte. (B and C) Colony formation assay. SK-N-BE cells were transfected with the indicated expression plasmids, and maintained in the culture medium containing 600 μg/ml of G418. Two weeks after the selection, drug-resistant colonies were stained with Giemsa's solution (B) and scored (C). (D and E) NLRR3-ICD enhances neurite elongation in response to ATRA. SK-N-BE cells stably expressing the indicated NLRR3 derivatives were maintained in the culture medium containing 1.5 μM of ATRA for 5 days and their images were taken through phase-contrast microscope. Scale bar; 200 μm (D). Histogram illustrates the percentage of neurite-bearing cells (E).

results were also obtained in the immunostaining experiments using anti-Tuj-1 antibody (Supplementary Fig. S1). Collectively, our present findings strongly suggest that the secretase-mediated proteolytic processing of NLRR3 to generate the COOH-terminal intracellular fragment and its subsequent nuclear access play a pivotal role in the regulation of ATRA-dependent neuroblastoma differentiation.

4. Discussion

It has been well-recognized that the therapeutic approach based on the induced differentiation of tumor cells is one of the most attractive strategies for malignant and aggressive tumor treatment. In this connection, a growing body of evidence demonstrated that retinoids have an ability to induce neuronal differentiation of neuroblastoma [19]. Indeed, ATRA-mediated differentiation of neuroblastoma cells has become a currently used therapeutic protocol. However, a precise molecular basis behind the neuroblastoma differentiation following ATRA exposure has been elusive. In this study, we have found for the first time that NLRR3, which is expressed higher in favorable neuroblastomas relative to unfavorable ones, participates in ATRA-induced neuroblastoma differentiation, and thus our present results might provide a novel insight into understanding ATRA-mediated biological responses such as differentiation.

One of the interesting findings of the present study is that the COOH-terminal intracellular domain of NLRR3 (NLRR3-ICD) is induced to be released from the plasma membrane and then accumulates in cell nucleus during ATRA-dependent differentiation of neuroblastoma SH-SY5Y cells. Indeed, ATRA-mediated nuclear access of NLRR3 in SH-SY5Y cells was massively attenuated in the presence of γ-secretase inhibitor as examined by immunostaining experiments (data not shown), and NLRR3-ICD production was significantly blocked by α- or γ-secretase inhibitor treatment, suggesting that ATRA-induced generation of NLRR3-ICD is regulated at least in part by secretase activities. In accordance with the previous findings showing that there are no distinct consensus amino acid sequences of intramembrane γ-cleavage sites among a broad range of its substrates [16], NLRR3 transmembrane domain also displayed no amino acid sequence similarity to those of Notch as well as the other γ-secretase substrates. However, the transmembrane domain of NLRR3 was highly conserved among human, mouse and rat (Fig. 2A), raising a possibility that γ-secretase-mediated liberation of the intracellular cytoplasmic domain of NLRR3 is evolutionarily conserved across mammalian species.

Meanwhile, it has been well-known that the released NICD directly moves from cytoplasm to nucleus, and then forms nuclear transcription complex with the sequence-specific DNA-binding protein CSL, Mastermind (MAM) family of transcriptional co-activators and/or transcriptional co-repressor MINT to transactivate and/or transrepress Notch-target genes [15]. According to our present observations, the exogenously expressed HA-NLRR3-ICD was translocated to cell nucleus, and also HA-NLRR3-ICD generated in SK-N-BE cells overexpressing HA-NLRR3 was detectable in nuclear fraction. Since we found out a canonical nuclear translocation signal (NLS) within NLRR3-ICD (RNYLQKPTFALGELYPP), it is possible that the nuclear access of NLRR3-ICD might be mediated by this putative NLS. Considering that Notch signaling results in the up-regulation and/or down-regulation of various Notch-target gene expression, it should be critical to investigate whether, like NICD, NLRR3-ICD could form active transcription complexes to regulate its target gene expression implicated in ATRA-mediated neuroblastoma differentiation.

As described [14], NLRR family consists of three members including NLRR1, NLRR2 and NLRR3. The close inspection of their transmembrane domains showed that there is no amino acid sequence similarity among them. Although a biological significance(s) of NLRR2 has remained to be determined, we have demonstrated that, in contrast to NLRR3, NLRR1 is expressed higher in unfavorable neuroblastomas as compared with that in favorable ones, and its expression level is correlated with poor prognosis of patients with neuroblastoma [13]. Subsequent studies revealed that *NLRR1* is a direct transcriptional target of MYCN and has an oncogenic potential [20]. Notably, there existed an inverse relationship between the expression levels of *NLRR3* and *MYCN* during ATRA-mediated neuroblastoma differentiation [14]. In support with this notion, forced expression and siRNA-mediated knockdown of *MYCN* resulted in a massive down- and up-regulation of *NLRR3* expression, respectively [14]. Based on our observations, it is likely that NLRR family such as NLRR1 and NLRR3 stands at the crossroad between MYCN-mediated oncogenic transformation and neuronal differentiation. Further studies should be required to adequately address this issue.

Taken together, our present findings strongly suggest that NLRR3-ICD generated by secretase-mediated proteolytic processing of NLRR3 contributes to ATRA-induced neuroblastoma differentiation, and might provide a clue to develop a novel therapeutic strategy for the treatment of aggressive neuroblastoma based on ATRA-induced differentiation.

Acknowledgments

This work was supported by a Grant-in-Aid from the Japan Ministry of Health, Labour and Welfare for Third Term Comprehensive Control Research for Cancer to A.N., JSPS KAKENHI Grant Number 21390317, 24249061 to A.N., 19890276 to A.T., MEXT KAKENHI Grant Number 22791016 to A.T.

Appendix A. Supplementary data

Supplementary data associated with this article can be found, in the online version, at http://dx.doi.org/10.1016/j.bbrc.2014.09.065.

References

[1] J.M. Maris, Recent advances in neuroblastoma, N. Engl. J. Med. 362 (2010) 2202–2211.
[2] G.M. Brodeur, A. Nakagawara, Molecular basis of clinical heterogeneity in neuroblastoma, Am. J. Pediatr. Hematol. Oncol. 14 (1992) 111–116.
[3] M.J. Cooper, S.M. Steinberg, J. Chatten, A.E. Evans, M.A. Israel, Plasticity of neuroblastoma tumor cells to differentiate along a fetal adrenal ganglionic lineage predicts for improved patient survival, J. Clin. Invest. 90 (1992) 2402–2408.
[4] A. Nakagawara, M. Arima-Nakagawara, N.J. Scavarda, C.G. Azar, B. Cantor, G.M. Brodeur, Association between high levels of expression of the TRK gene and favorable outcome in human neuroblastoma, N. Engl. J. Med. 328 (1993) 847–854.
[5] V.R. Ganeshan, N.F. Schor, Pharmacologic management of high-risk neuroblastoma in children, Paediatr. Drugs 13 (2011) 245–255.
[6] J. Hara, Development of treatment strategies for advanced neuroblastoma, Int. J. Clin. Oncol. 17 (2012) 196–203.
[7] D. Meitar, S.E. Crawford, A.W. Rademaker, S.L. Cohn, Tumor angiogenesis correlates with metastatic disease, N-myc amplification, and poor outcome in human neuroblastoma, J. Clin. Oncol. 14 (1996) 405–414.
[8] J.M. Maris, K.K. Matthay, Molecular biology of neuroblastoma, J. Clin. Oncol. 17 (1999) 2264–2279.
[9] G.P. Tonini, Neuroblastoma: the result of multistep transformation?, Stem Cells 11 (1993) 276–282
[10] R. Ijiri, Y. Tanaka, K. Kato, K. Misugi, H. Nishihira, Y. Toyoda, H. Kigasawa, T. Nishi, M. Takeuchi, N. Aida, T. Momoi, Clinicopathologic study of mass-screened neuroblastoma with special emphasis on untreated observed cases: a possible histologic clue to tumor regression, Am. J. Surg. Pathol. 24 (2000) 807–815.
[11] G. López-Carballo, L. Moreno, S. Masiá, P. Pérez, D. Barettino, Activation of the phosphatidylinositol 3-kinase/Akt signaling pathway by retinoic acid is required for neural differentiation of SH-SY5Y human neuroblastoma cells, J. Biol. Chem. 277 (2002) 25297–25304.
[12] M. Ohira, A. Morohashi, H. Inuzuka, T. Shishikura, T. Kawamoto, H. Kageyama, Y. Nakamura, E. Isogai, H. Takayasu, S. Sakiyama, Y. Suzuki, S. Sugano, T. Goto, S. Sato, A. Nakagawara, Expression profiling and characterization of 4200

genes cloned from primary neuroblastomas: identification of 305 genes differentially expressed between favorable and unfavorable subsets, Oncogene 22 (2003) 5525–5536.
[13] S. Hamano, M. Ohira, E. Isogai, K. Nakada, A. Nakagawara, Identification of novel human neuronal leucine-rich repeat (hNLRR) family genes and inverse association of expression of Nbla10449/hNLRR-1 and Nbla10677/hNLRR-3 with the prognosis of primary neuroblastomas, Int. J. Oncol. 24 (2004) 1457–1466.
[14] J. Akter, A. Takatori, M.S. Hossain, T. Ozaki, A. Nakazawa, M. Ohira, Y. Suenaga, A. Nakagawara, Expression of NLRR3 orphan receptor gene is negatively regulated by MYCN and Miz-1, and its downregulation is associated with unfavorable outcome in neuroblastoma, Clin. Cancer Res. 17 (2011) 6681–6692.
[15] K. Hori, A. Sen, S. Artavanis-Tsakonas, Notch signaling at a glance, J. Cell Sci. 126 (2013) 2135–2140.
[16] B. De Strooper, Aph-1, Pen-2, and Nicastrin with Presenilin generate an active gamma-Secretase complex, Neuron 38 (2003) 9–12.
[17] G.H. Searfoss, W.H. Jordan, D.O. Calligaro, E.J. Galbreath, L.M. Schirtzinger, B.R. Berridge, H. Gao, M.A. Higgins, P.C. May, T.P. Ryan, Adipsin, a biomarker of gastrointestinal toxicity mediated by a functional gamma-secretase inhibitor, J. Biol. Chem. 278 (2003) 46107–46116.
[18] S.E. Hoey, R.J. Williams, M.S. Perkinton, Synaptic NMDA receptor activation stimulates alpha-secretase amyloid precursor protein processing and inhibits amyloid-beta production, J. Neurosci. 29 (2009) 4442–4460.
[19] M. Ponzoni, P. Bocca, V. Chiesa, A. Decensi, V. Pistoia, L. Raffaghello, C. Rozzo, P.G. Montaldo, Differential effects of *N*-(4-hydroxyphenyl)retinamide and retinoic acid on neuroblastoma cells: apoptosis versus differentiation, Cancer Res. 55 (1995) 853–861.
[20] M.S. Hossain, T. Ozaki, H. Wang, A. Nakagawa, H. Takenobu, M. Ohira, T. Kamijo, A. Nakagawara, N-MYC promotes cell proliferation through a direct transactivation of neuronal leucine-rich repeat protein-1 (NLRR1) gene in neuroblastoma, Oncogene 27 (2008) 6075–6082.

Cell

Premature Termination of Reprogramming In Vivo Leads to Cancer Development through Altered Epigenetic Regulation

Kotaro Ohnishi,[1,2,8] Katsunori Semi,[1,3,8] Takuya Yamamoto,[1,3] Masahito Shimizu,[2] Akito Tanaka,[1] Kanae Mitsunaga,[1] Keisuke Okita,[1] Kenji Osafune,[1] Yuko Arioka,[1] Toshiyuki Maeda,[4] Hidenobu Soejima,[4] Hisataka Moriwaki,[2] Shinya Yamanaka,[1,3,5] Knut Woltjen,[1,6] and Yasuhiro Yamada[1,3,7,*]

[1]Center for iPS Cell Research and Application (CiRA), Kyoto University, Kyoto 606-8507, Japan
[2]Department of Medicine, Gifu University Graduate School of Medicine, Gifu 501-1194, Japan
[3]Institute for Integrated Cell-Material Sciences (WPI-iCeMS), Kyoto University, Kyoto 606-8507, Japan
[4]Division of Molecular Genetics and Epigenetics, Department of Biomolecular Sciences, Faculty of Medicine, Saga University, Saga 849-8501, Japan
[5]Gladstone Institute of Cardiovascular Disease, San Francisco, CA 94158, USA
[6]Hakubi Center for Advanced Research, Kyoto University, Kyoto 606-8507, Japan
[7]PRESTO, Japan Science and Technology Agency, 4-1-8 Honcho Kawaguchi, Saitama, 332-0012, Japan
[8]These authors contributed equally to this work
*Correspondence: y-yamada@cira.kyoto-u.ac.jp
http://dx.doi.org/10.1016/j.cell.2014.01.005

SUMMARY

Cancer is believed to arise primarily through accumulation of genetic mutations. Although induced pluripotent stem cell (iPSC) generation does not require changes in genomic sequence, iPSCs acquire unlimited growth potential, a characteristic shared with cancer cells. Here, we describe a murine system in which reprogramming factor expression in vivo can be controlled temporally with doxycycline (Dox). Notably, transient expression of reprogramming factors in vivo results in tumor development in various tissues consisting of undifferentiated dysplastic cells exhibiting global changes in DNA methylation patterns. The Dox-withdrawn tumors arising in the kidney share a number of characteristics with Wilms tumor, a common pediatric kidney cancer. We also demonstrate that iPSCs derived from Dox-withdrawn kidney tumor cells give rise to nonneoplastic kidney cells in mice, proving that they have not undergone irreversible genetic transformation. These findings suggest that epigenetic regulation associated with iPSC derivation may drive development of particular types of cancer.

INTRODUCTION

Induced pluripotent stem cells (iPSCs) can be established from differentiated somatic cells by the forced induction of four transcription factors: *Oct3/4*, *Klf4*, *Sox2*, and *c-Myc* (Takahashi et al., 2007; Takahashi and Yamanaka, 2006; Maherali et al., 2007; Okita et al., 2007; Wernig et al., 2007; Woltjen et al., 2009). To achieve somatic cell reprogramming, multiple cellular processes act synergistically in a sequential manner (Brambrink et al., 2008; Polo et al., 2012; Samavarchi-Tehrani et al., 2010). Despite extensive studies, the precise mechanism of somatic cell reprogramming still remains unclear (Rais et al., 2013). It is known that non-iPSC-like colonies often appear at the intermediate stage of cellular reprogramming in vitro. In addition, there are several reports describing partial iPSCs that deviate successful reprogramming (Fussner et al., 2011; Mikkelsen et al., 2008; Sridharan et al., 2009). However, the characteristics of such failed reprogramming states are largely unknown, and no study has elucidated the failed reprogramming state from cell types other than fibroblasts.

The process of iPSC derivation shares many characteristics with cancer development. During reprogramming, somatic differentiated cells acquire the properties of self-renewal along with unlimited proliferation and exhibit global alterations of the transcriptional program, which are also critical events during carcinogenesis (Ben-Porath et al., 2008). The metabolic switch to glycolysis that occurs during somatic cell reprogramming is similarly observed in cancer development (Folmes et al., 2011). Such similarities suggest that reprogramming processes and cancer development may be partly promoted by overlapping mechanisms (Hong et al., 2009). Practically, the forced induction of the critical reprogramming factor *Oct3/4* in adult somatic cells results in dysplastic growth in epithelial tissues through the inhibition of cellular differentiation in a manner similar to that in embryonic cells (Hochedlinger et al., 2005). These studies provided a possible link between transcription-factor-mediated reprogramming and cancer development.

To elucidate the involvement of failed reprogramming in cancer development, in the present study, we generated an in vivo reprogramming mouse system using reprogramming factor-inducible alleles and examined the effects of reprogramming factor expression in somatic cells in vivo. We show that failed reprogramming-associated cells behave similarly to cancer cells

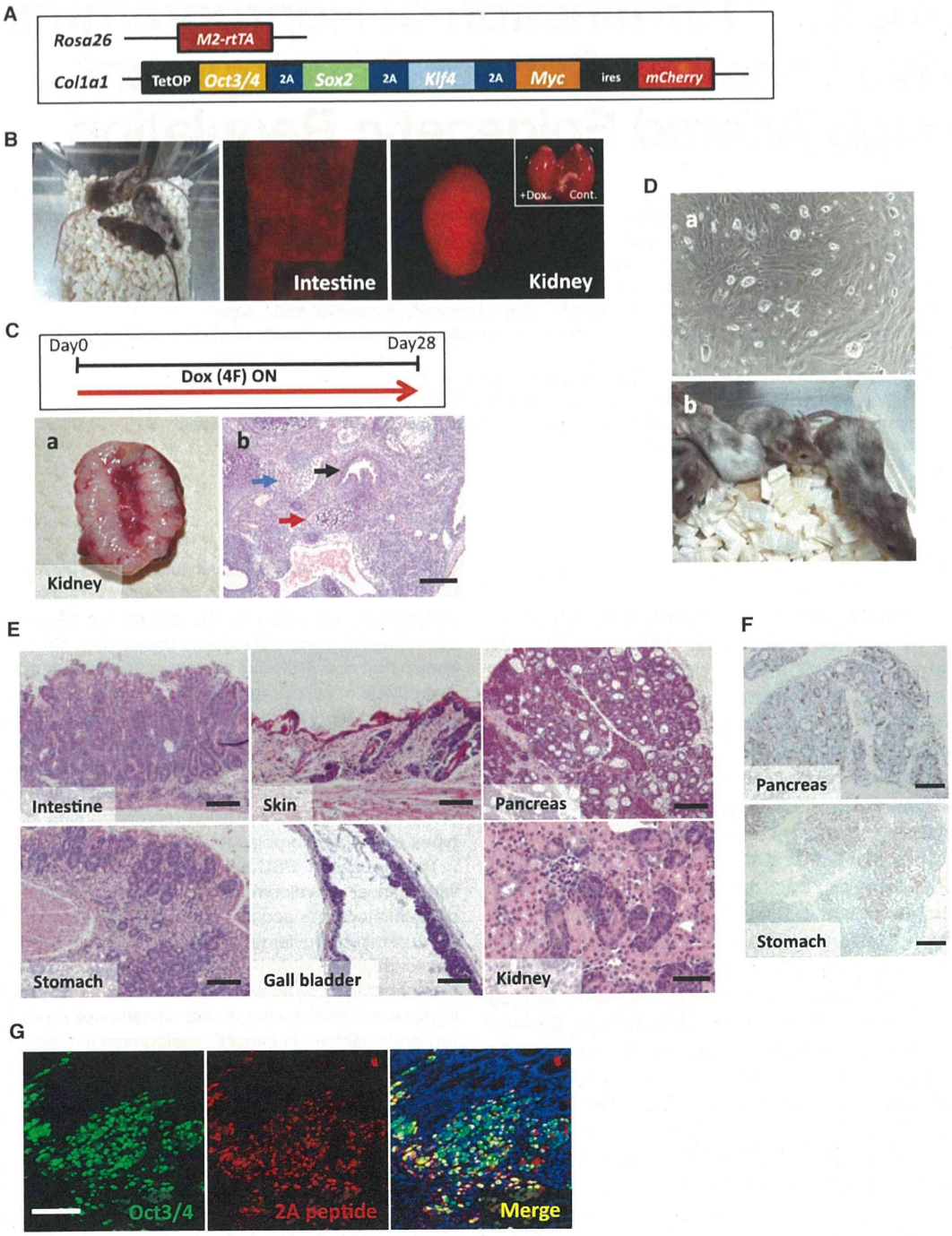

Figure 1. Reprogramming of Somatic Cells In Vivo

(A) Generation of four-factor-inducible ESCs. TetOP, tetracycline-dependent promoter.

(B) Generation of chimeric mice using OSKM-inducible ESCs. mCherry signals could be detected in various organs after Dox treatment for 3 days.

(C) Treatment of chimeric mice with Dox for 28 days resulted in the development of multiple tumors containing pluripotent stem cells. (a) A representative macroscopic image of the cut surface of the kidney tumor. (b) A histological section of the kidney tumor showing the differentiation of tumor cells into three germ layers, indicating teratoma formation. The blue, red, and black arrows represent neuronal, cartilage, and glandular epithelial components, respectively. Scale bar, 200 μm.

(legend continued on next page)

and cause neoplasia resembling Wilms tumor, a childhood blastoma in the kidney. Moreover, we demonstrate that altered epigenetic regulations cause the abnormal growth of such failed reprogramming-associated cancer cells.

RESULTS

In Vivo Reprogrammable Mouse

To establish the reprogrammable mouse system, we generated embryonic stem cells (ESCs) in which reprogramming factors can be induced under the control of doxycycline (Dox) (Figure 1A) (Carey et al., 2010; Stadtfeld et al., 2010b). We used KH2 ESCs with the optimized reverse tetracycline-dependent transactivator at the *ROSA 26* locus (Beard et al., 2006). A polycistronic cassette encoding four reprogramming factors (*Oct3/4*, *Sox2*, *Klf4*, and c-*Myc*) (Carey et al., 2010), followed by *ires-mCherry*, was targeted into the *Col1a1* gene locus under the tetracycline-dependent promoter of KH2 ESCs (Figure 1A).

Next, we generated chimeric mice via blastocyst injection of four-factor (4F)-inducible ESCs. To confirm inducible expression of the reprogramming factors and mCherry in vivo, Dox-containing water was provided to chimeric mice starting at 4 weeks of age. On day 3 of Dox treatment, we could detect the mCherry signal in various organs, including stomach, intestine, liver, pancreas, kidney, gallbladder, and skin (Figure 1B). We also confirmed the expression of reprogramming factors in germline-transmitted mouse tissues by quantitative RT-PCR (qRT-PCR) (Figure S1A available online).

Mouse embryonic fibroblasts (MEFs) containing these reprogramming factor-inducible alleles could give rise to iPSCs after Dox treatment in vitro (Figure S1B). We next asked whether responding somatic cells could be reprogrammed in vivo. The chimeric and germline-transmitted mice given Dox-containing water (2 mg/ml) from 4 weeks of age became morbid within 7–10 days and a few days, respectively. A small proportion of chimeric mice could be treated with Dox for 4 weeks, presumably because of a lower contribution of ESCs in responding tissues. Notably, mice treated with Dox for 4 weeks developed multiple tumors in several organs, such as the kidney and pancreas (Figure 1Ca), whereas tumor formation was never observed in nontreated mice (n = 7, 7 months of age). Histological analysis revealed that these tumors differentiated into three different germ layers, indicating that they are teratomas (Figure 1Cb). When teratoma cells were cultured ex vivo in the absence of Dox (no additional 4F expressions), iPSC-like cells were established (Figure 1Da). Importantly, the teratoma-derived iPSC-like cells contributed to adult chimeric mice when they were injected into blastocysts (Figure 1Db). Therefore, we conclude that somatic cells can be reprogrammed in vivo to pluripotency in our reprogrammable mouse system.

Forced Expression of Reprogramming Factors In Vivo Leads to Rapid Expansion of Dysplastic Cells

We next examined the early changes after expression of reprogramming factors in somatic cells in vivo. After treatment of 4-week-old mice with Dox for 3–9 days, all mice developed dysplastic lesions in epithelial tissues of various organs (Figure 1E), although there were variations in severity of the phenotype among chimeras. Dysplastic cells proliferated actively, as revealed by Ki67 staining (Figure 1F). Abnormal proliferation of somatic cells was observed as early as 3 days after Dox treatment (Figure S1C), and by day 7, such dysplastic cell growth was detected even for pancreatic and kidney cells, which typically do not divide actively under physiological conditions (Figures 1E and 1F). Immunofluorescent analysis of Oct3/4 and the 2A peptide (forming transgene connections) demonstrated that the dysplastic cells expressed reprogramming factors (Figure 1G). Collectively, the forced expression of reprogramming factors caused dysplastic cell expansion of epithelial tissues in vivo.

The Fate of Early Dysplastic Cells after Withdrawal of Dox

To examine whether subsequent expansion of such dysplastic cells depends on the continuous expression of reprogramming factors, we withdrew Dox for 7 days after an initial 4- to 7-day treatment (Figure 2A). Although Dox treatment for 4–7 days caused active cell proliferation in a variety of tissues of all mice, we did not observe any dysplastic cells in some mice after withdrawal of Dox (Figure 2A; Table 1). Of particular note, mice treated with Dox for periods less than 5 days before withdrawal often revealed a lack of dysplastic cells (Table 1). These data suggest that early dysplastic cell growth requires continuous expression of reprogramming factors. We next investigated the fate of eliminated dysplastic proliferating cells after the withdrawal of Dox. Bromodeoxyuridine (BrdU) was injected into mice during Dox treatment to label proliferating cells caused by reprogramming factor expression during the first 7 days (Hochedlinger et al., 2005), and then mice were sacrificed after the withdrawal of Dox for 7 days, on day14. Notably, BrdU-labeled cells were often observed in normal-looking pancreatic and kidney tissues at day14 (Figure 2B). Furthermore, BrdU-labeled cells in the pancreatic islets also expressed insulin (Figure 2B). This suggests that the expanded cells caused by the transient expression of reprogramming factors were, at least in part, integrated into normal-looking tissues after Dox withdrawal.

(D) Teratomas contain pluripotent stem cells. (a) Ex vivo teratoma culture gave rise to iPSC-like colonies without Dox exposure. (b) Teratoma-derived iPSCs contributed to adult chimeric mice.

(E) Dysplastic cell expansion by the forced expression of reprogramming factors in vivo. The histology of various organs of mice treated with Dox for 3 to 9 days. Scale bars, 200 μm (intestine, skin, pancreas, stomach, and gall bladder) and 100 μm (kidney).

(F) Ki67 immunostaining revealed active proliferation of the dysplastic cells in the pancreas and stomach. Scale bars, 200 μm.

(G) Immunofluorescent staining for Oct3/4 and 2A peptide in the intestine of an OSKM chimeric mouse treated with Dox for 7 days. The 2A antibody used here recognizes both Oct3/4-P2A and Sox2-T2A. Dysplastic cells showed positive staining for both Oct3/4 and 2A. Scale bar, 50 μm.

See also Figure S1.